SUPPLEMENTAL MATERIAL

for the manuscript by

Kazuo Yamasaki, Guoli Wang, Takashi Daiho, Stefania Danko, and Hiroshi Suzuki

Roles of Tyr^{122}-Hydrophobic Cluster and K^+ Binding in Ca^{2+}-releasing Process of ADP-insensitive Phosphoenzyme of Sarcoplasmic Reticulum Ca^{2+}-ATPase

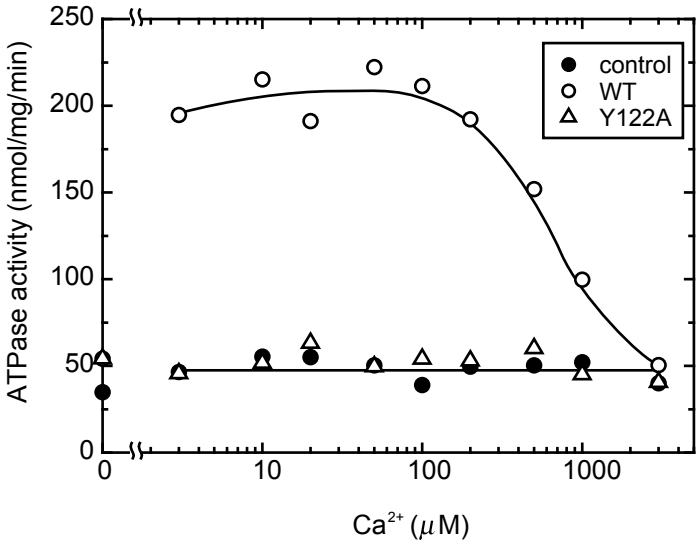

Supplemental Figure 1

Supplemental Figure 1. **ATPase activities of SERCA1a wild type and mutant Y122A at various high concentrations of Ca^{2+}.** The ATPase activities of the microsomes expressing SERCA1a wild type (WT) or mutant Y122A, and that of the control microsomes (no SERCA1a expression) were determined at various Ca^{2+} concentrations in the presence of A23187 and 7 mM $MgCl_2$ as described under "EXPERIMENTAL PROCEDURES." The points at zero Ca^{2+} indicate the activities determined without the $CaCl_2$ addition. Note that the Ca^{2+}-ATPase activity was completely inhibited in Y122A at all the Ca^{2+} concentrations. In the wild type, the reduction of the activity at the high Ca^{2+} concentrations involves not only the lumenal Ca^{2+}-induced feedback inhibition but also the marked retardation of the Ca^{2+}-ATPase cycle by the substrate CaATP produced at the high Ca^{2+} concentrations. In fact, the affinity of the enzyme for CaATP is approximately 10 times higher than that for MgATP, and the turnover rate of *E*P formed from CaATP (thus Ca^{2+} bound at the catalytic site) is far slower than that formed with MgATP (41). Therefore, even with the wild type, it is not possible to determine the lumenal Ca^{2+} affinity by this experimental design.

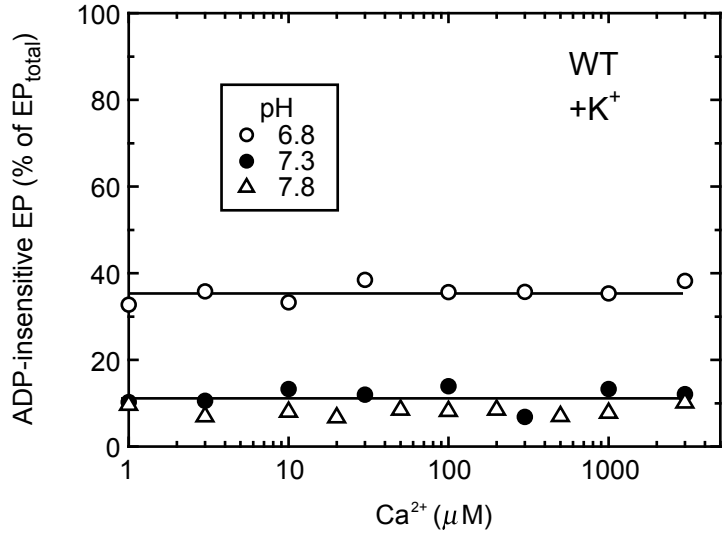

Supplemental Figure 2

Supplemental Figure 2. **Ca^{2+} dependence of accumulation of ADP-insensitive *E*P in the steady state in wild type.** The fraction of ADP-insensitive *E*P in the total amount of *E*P was determined with the wild type at various Ca^{2+} concentrations as described in Fig. 2 for the mutant Y122A.

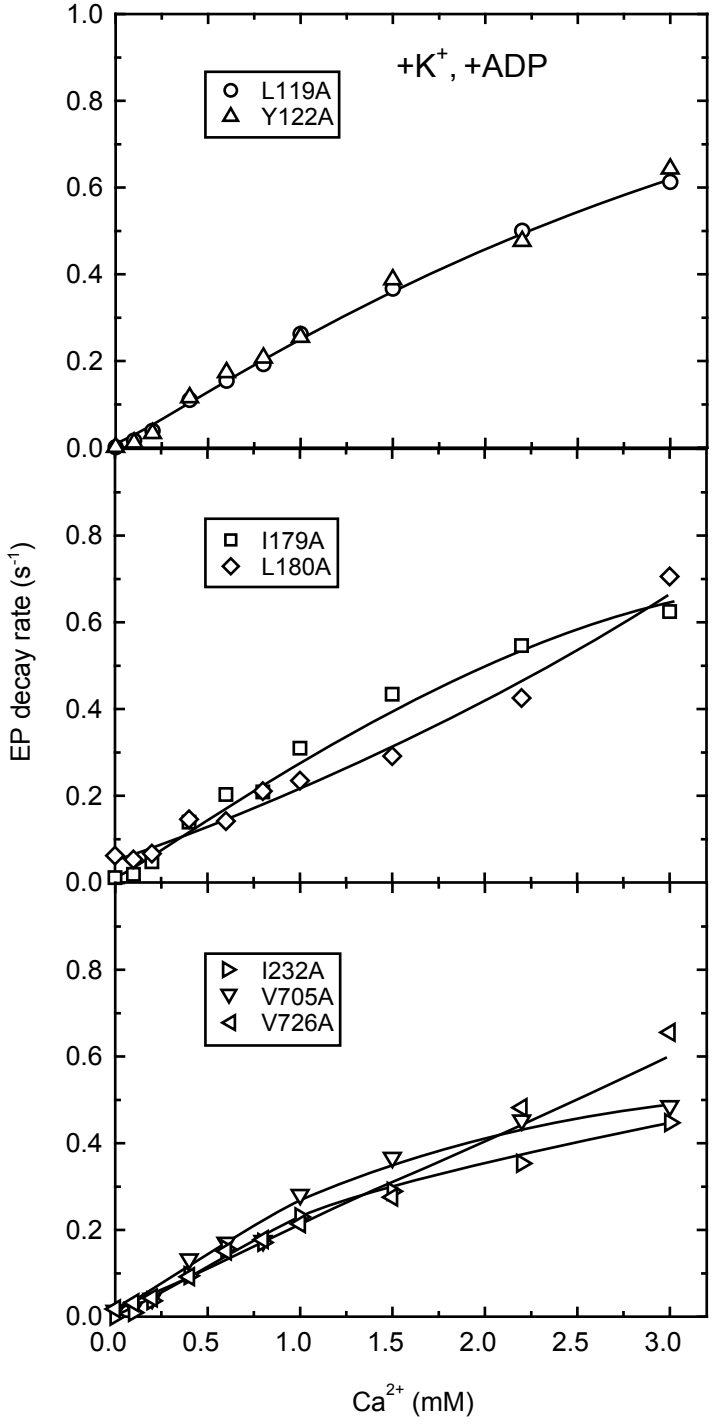

Supplemental Figure 3

Supplemental Figure 3. **Lumenal Ca^{2+}- and ADP-induced reverse *E*2P decay of Tyr^{122}-hydrophobic cluster mutants in the presence of K^+.** With all the seven Y122-HC mutants, *E*2P was first formed from $^{32}P_i$ in the absence of Ca^{2+}, and the *E*2P decay time courses upon the addition of various concentrations of Ca^{2+} and ADP were determined as described in Fig. 7*A* for the representative mutant Y122A. The single exponential decay rates thus obtained were plotted *versus* Ca^{2+} concentrations as in Fig. 7*B*.

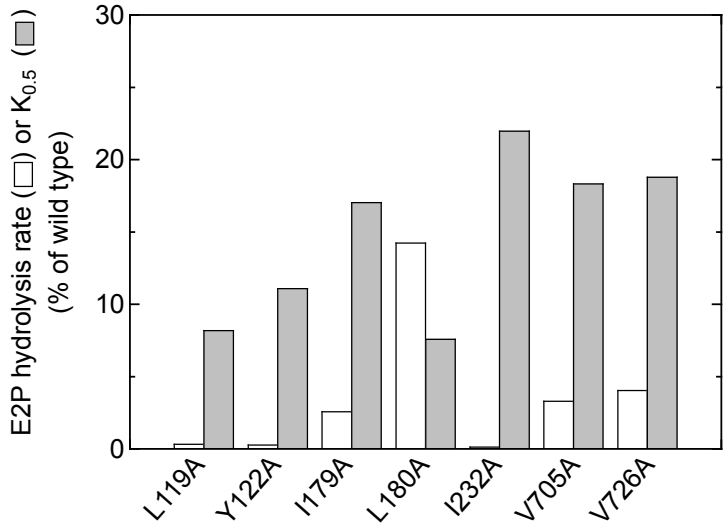

Supplemental Figure 4

Supplemental Figure 4. **Different extents of mutational effects of seven residues in Y122-HC on *E2*P hydrolysis and lumenal Ca^{2+} affinity.** The *E*2P hydrolysis rates of each of the seven mutants for Y122-HC (*open bars*) were determined in the absence of Ca^{2+} and ADP and presence of 0.1 M K^+ otherwise as in Fig. 7. The results agree with our previous study (22). The apparent affinities of *E*2P for lumenal Ca^{2+} in the presence of 0.1 M K^+ at pH 7.3 ($K_{0.5}$, *gray bars*) were determined with the seven Y122-HC mutants in Fig. 6 and estimated with the wild type in Fig. 8*B*. These values are shown as % of those of the wild type.

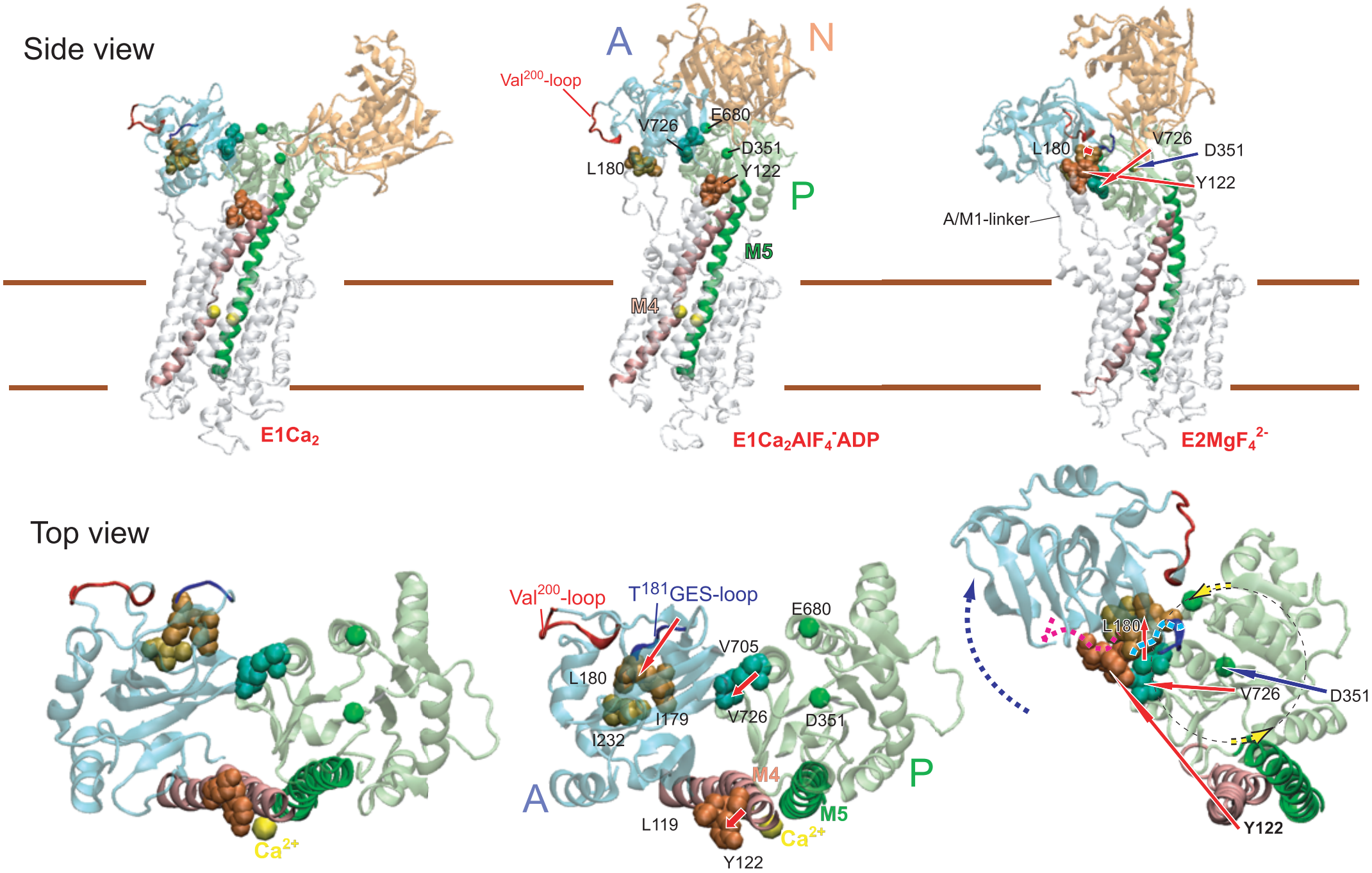

Supplemental Figure 5A

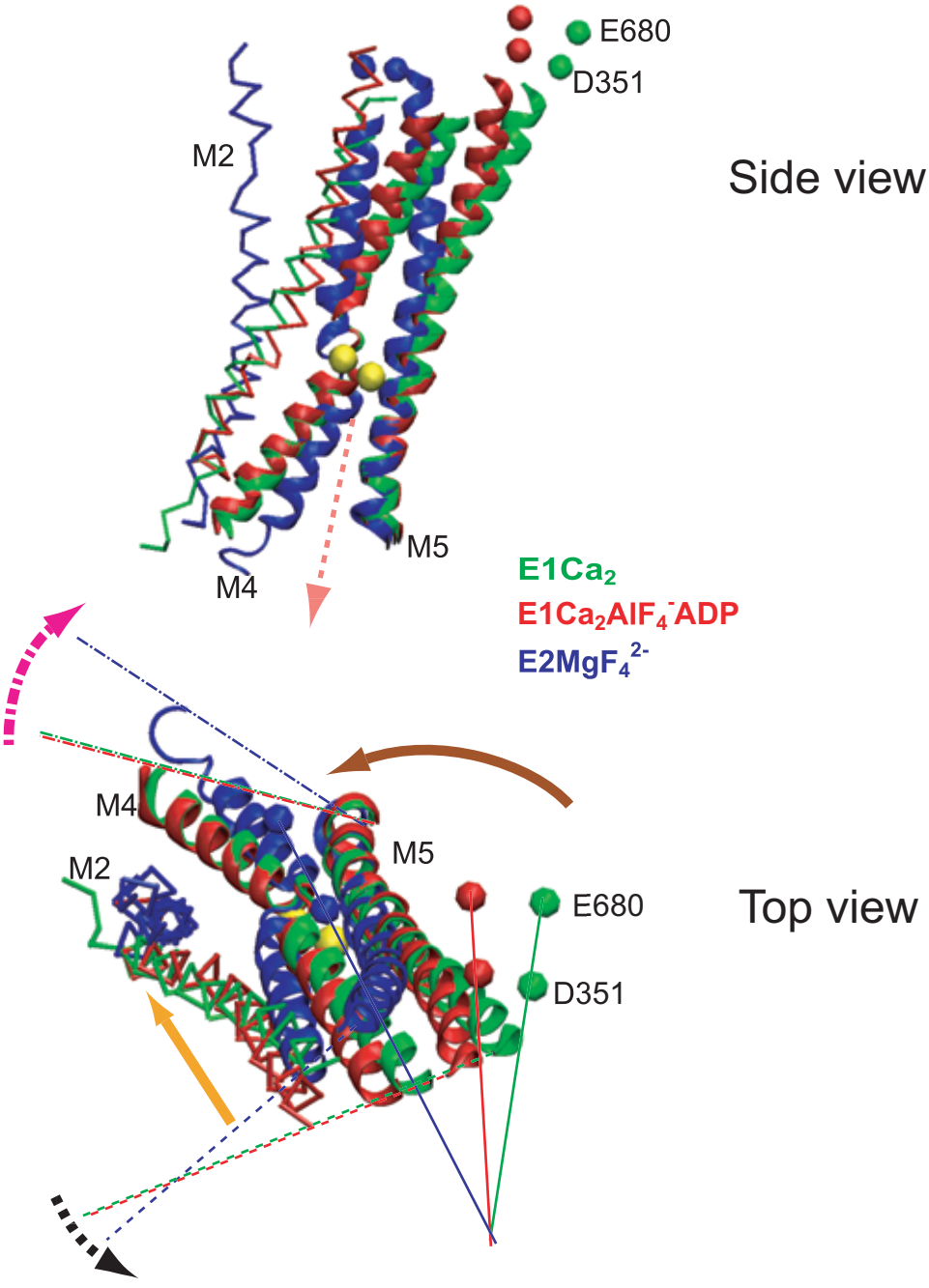

Supplemental Figure 5B

Supplemental Figure 5. **Inclination and rotational movements of P domain with twisting-like motion of M4 and M5 in *E*1PCa$_2$ → *E*2P + 2Ca^{2+}.** Three structures *E*1Ca$_2$ (PDB code; 1SU4 (10)), *E*1Ca$_2$·AlF$_4^-$·ADP (the analog for transition state *E*1~PCa$_2$·ADP (1T5T (12))), and *E*2·MgF$_4^{2-}$ (*E*2·P$_i$ analog (1WPG)) are fitted manually with M8-M10 helices.

(*A*) *Side view* of the whole molecule and *Top view* of the P and A domains, M4, and M5 from the cytoplasmic side are shown by semitransparent mode. The seven residues involved in Y122-HC (Leu^{119}/Tyr^{122}, Ile^{179}/Leu^{180}, Ile^{232}, and Val^{705}/Val^{726}) are shown by *van der Waals spheres*. The Val^{200} loop and T^{181}GES loop are depicted by *ribbon diagrams*. The alpha carbons of Asp^{351} (located approximately at the center of the P domain) and Glu^{680} (at the outermost part of this domain) were depicted by *green spheres* to show the motion of the P domain. The three *thin red arrows* on *Top view* of *E*1Ca$_2$·AlF$_4^-$·ADP show the movements of Tyr^{122}, Leu^{180}, and Val^{726}, respectively, from *E*1Ca$_2$ to *E*1Ca$_2$·AlF$_4^-$·ADP. The three *thin red arrows* on the *Side* and *Top views* of *E*2·MgF$_4^{2-}$ show the movements of these three residues from *E*1Ca$_2$·AlF$_4^-$·ADP to *E*2·MgF$_4^{2-}$ (as indicated by Y122, L180, and V726) to form Y122-HC. The *solid blue arrow* on *E*2·MgF$_4^{2-}$ shows the movement of Asp^{351} from *E*1Ca$_2$·AlF$_4^-$·ADP to *E*2·MgF$_4^{2-}$. The *dotted yellow arc arrows* on *E*2·MgF$_4^{2-}$ show the rotational motion of the P domain around Asp^{351} in the change from *E*1Ca$_2$·AlF$_4^-$·ADP to *E*2·MgF$_4^{2-}$; note that the *dotted yellow arc arrow* placed on Glu^{680} (*green sphere*) actually indicates the approximate movement of this residue in the change. In *E*2·MgF$_4^{2-}$, Glu^{680} is located in the immediate vicinity of the Val^{200} loop and actually involved in the ionic interactions with this loop. The *dotted blue arc arrow* on *E*2·MgF$_4^{2-}$ shows the rotational movement of A domain from *E*1Ca$_2$·AlF$_4^-$·ADP to *E*2·MgF$_4^{2-}$ around the T^{181}GES-loop region. The *dotted pink* and *light blue ribbons* superimposed on *E*2·MgF$_4^{2-}$ indicate the locations of the Val^{200}- and T^{181}GES-loops in *E*1Ca$_2$·AlF$_4^-$·ADP, respectively; the Val^{200} loop, the outermost loop of the A domain, largely moves and comes to the interface with the P domain at Glu^{680} as the A domain largely rotates around the T^{181}GES-loop region.

(*B*) M4 and M5 (*solid ribbons*), M2 (*trace of its alpha carbons*), and the alpha carbons of Asp^{351} and Glu^{680} (*van der Waals spheres*) are exhibited in the three structures; *E*1Ca$_2$ (*green*), *E*1Ca$_2$·AlF$_4^-$·ADP (*red*), and *E*2·MgF$_4^{2-}$ (*blue*). The three structures are fitted manually with M8-M10. The *Side view* and *Top view* from the cytoplasmic side are shown. The two Ca^{2+} ions bound in *E*1Ca$_2$·AlF$_4^-$·ADP are shown by *yellow van der Waals spheres*, and its release into lumen is roughly shown by *dotted salmonpink arrow* on *Side view*. On *Top view*, the three *thin solid lines* are drawn from Glu^{680} (the outermost part of the P domain) through Asp^{351} (the approximate center of the P domain) to show their alignment in each of the three structures and thus to depict the rotational motion of the P domain (*brown solid arc arrow*) in the change from *E*1Ca$_2$ to *E*1Ca$_2$·AlF$_4^-$·ADP and further to *E*2·MgF$_4^{2-}$. The three *broken thin lines* are drawn from the cytoplasmic top part of M5 (Phe^{740}) through that of M4 (Lys^{329}), and three *dash-dotted thin lines* are from the lumenal end of M5 (Leu^{781}) through that of M4 (Ile^{289}). These two sets of the three lines are to depict the motions of M4 and M5 at the cytoplasmic part (*black broken arc arrow*) and at the lumenal end (*magenta dash-dotted arc arrow*) in the change

from $E1Ca_2$/$E1Ca_2$·AlF_4^-·ADP to $E2{\cdot}MgF_4^{2-}$. The *orange solid arrow* shows the movement of Tyr^{122} on the cytoplasmic top part of M2 in the change from $E1Ca_2$/$E1Ca_2$·AlF_4^-·ADP to $E2{\cdot}MgF_4^{2-}$.

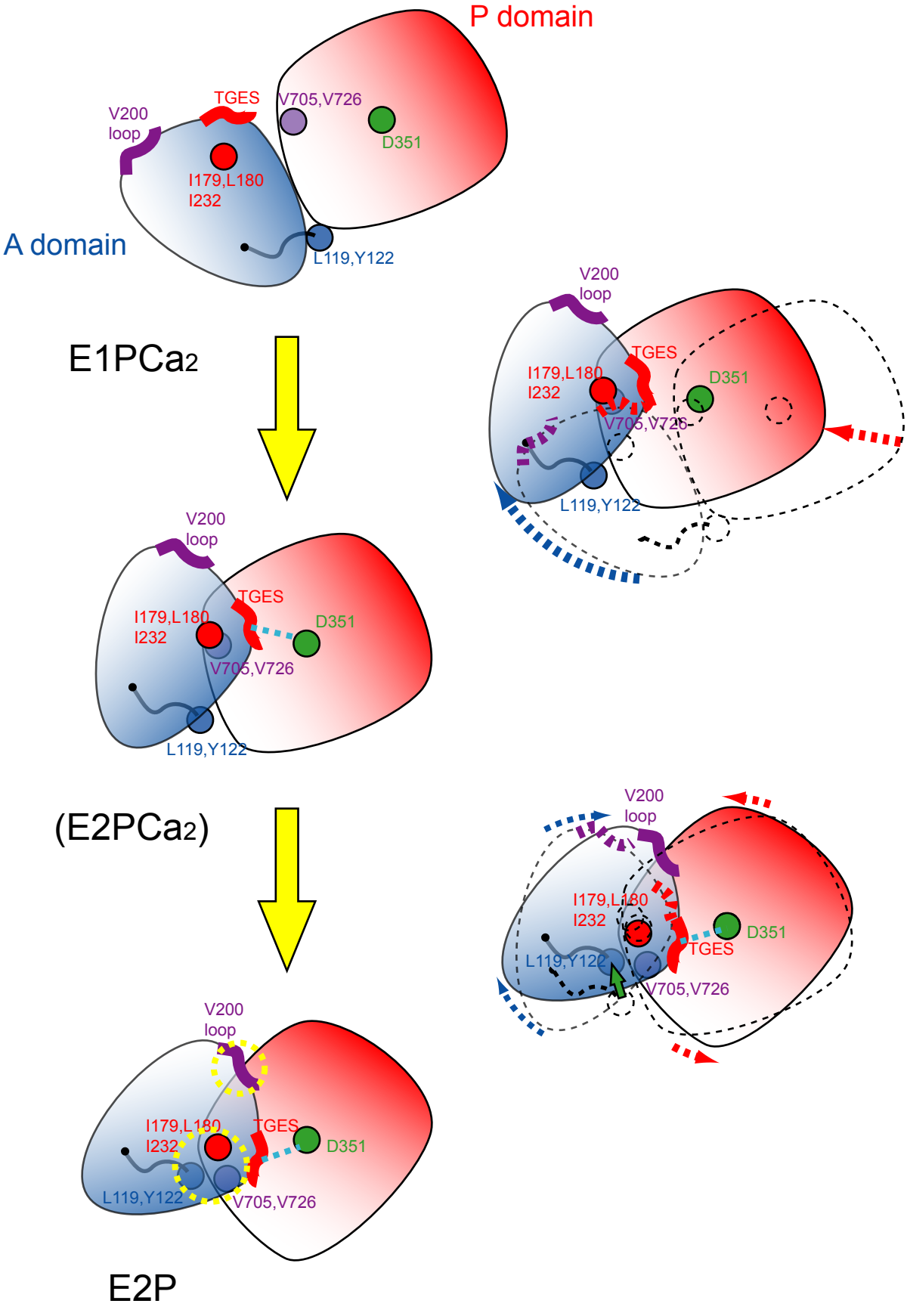

Supplemental Figure 6

Supplemental Figure 6. **Schematic model for rearrangement of P and A domains for *E*P isomerization and Ca^{2+} release**. Depicted is our schematic model for the motions of the A and P domains in the successive two steps (*large yellow arrows*); *E*1PCa_2 → *E*2PCa_2 (loss of the ADP-sensitivity) and *E*2PCa_2 → *E*2P + $2Ca^{2+}$ (Ca^{2+} release). The model is made on the basis of the observed mutational effects of Y122-HC and Val^{200} loop (22-24). The top view from the cytoplasmic side is shown (as in *Top view* of Supplemental Figure 3A). The P and A domains, Val^{200} loop, T^{181}GES loop, and Asp^{351} in *E*1PCa_2 and *E*2P are positioned according to the structures of *E*1Ca_2·AlF_4^-·ADP (1T5T) and *E*2·MgF_4^{2-} (1WPG), respectively. *E*2PCa_2 is the postulated intermediate state. The positions of the seven residues involved in Y122-HC in the three regions are shown by the representative ones (Y122, L180, and V705). In the pictures placed for the two *large yellow arrows*, the structure (*broken lines*) before its change was superimposed on that after the change, and the motions of the A and P domains are indicated by *dotted blue arrow* and *dotted red arrow*, respectively.

*E*1PCa_2 → *E*2PCa_2; the loss of ADP-sensitivity:

The A domain rotates largely (probably due to the strain of the A/M3-linker) around the T^{181}GES loop and the P domain inclines to some extent toward the A domain, thereby the T^{181}GES loop docks onto the Asp^{351}-region producing hydrogen-bonding interactions (*dotted blue line*), hence causing the loss of the ADP-sensitivity (the T^{181}GES loop blocks the access of ADP *β*-phosphate to Asp^{351}-acylphosphate). In this state, the two interaction networks at Y122-HC and at the Val^{200} loop are not yet fully produced. Our previous mutation study on the interaction network between Arg^{334}/Arg^{324} of the P domain and top part of M2 (Glu^{123}/Tyr^{122}/Glu^{121}/Glu^{117}/Asn^{114}/Glu^{113}/Asn^{111}/Glu^{109}/Gln^{108}) indicated (22) that the inclination of the P domain occur at least to some extent along this interaction network for the loss of the ADP-sensitivity, *E*1PCa_2 → *E*2PCa_2.

*E*2PCa_2 → *E*2P + $2Ca^{2+}$; Ca^{2+} release after the loss of ADP-sensitivity:

The P and A domains further rotate slightly in the opposite directions and the top part of M2 (Tyr^{122}/Leu^{119}) likely moves more (*green solid arrow*), thereby they produce the interactions fully at Y122-HC and at Val^{200} loop (*dotted yellow circles*) so as to realize and stabilize the Ca^{2+}-released structure of *E*2P. The native and appropriately short length of the A/M1-linker (its strain) critically contributes to the structural changes for Ca^{2+}-deocclusion/release and formation of Y122-HC in *E*2PCa_2 → *E*2P + $2Ca^{2+}$; in this case, especially for the vertical motions of the P and A domains and M4/M5, and the inclination of M2. These vertical factors are not depicted in this top view.

Upon these changes, the catalytic site is rearranged to produce its appropriate configuration for the subsequent Asp^{351}-acylphosphate hydrolysis, *e.g.* the T^{181}GES loop comes to the position where the Glu^{183}-coordinated water molecule can attack Asp^{351}-acylphosphate. Hence in this structural mechanism, the possible hydrolysis without releasing Ca^{2+} is avoided, and the Ca^{2+} release and the subsequent *E*2P hydrolysis are accomplished as the ordered sequence.

In the wild type, all these successive structural events in *E*1PCa_2 → *E*2PCa_2 → *E*2P + $2Ca^{2+}$ occur in coordinated manner and thus rapidly; therefore *E*2PCa_2 does not accumulate stably in the wild type.